Stem Cell Research & Therapy

RESEARCH

Open Access

Activation of eIF2*α*-ATF4 by endoplasmic reticulum-mitochondria coupling stress enhances COX2 expression and MSC-based therapeutic efficacy for rheumatoid arthritis

Jiaqing Liu[1†], Xing Zhang[1†], Xiangge Zhao[1], Jinyi Ren[1], Huina Huang[1], Cheng Zhang[1], Xianmei Chen[1], Weiping Li[2*], Jing Wei[1*] and Xia Li[1*]

Abstract

Background Mesenchymal stem/stromal cell (MSC) therapy holds promise as a therapeutic strategy for rheumatoid arthritis (RA). However, the loss of secretory function following cell delivery has significantly restricted its clinical application. Our preliminary studies confirmed that endoplasmic reticulum stress (ERS)-MSCs greatly inhibited RA follicular helper T cells (Tfh) through cyclooxygenase-2 (COX2)/prostaglandin E2 (PGE2) pathway activation via an unknown molecular mechanism, demonstrating the therapeutic effects of ERS-modified MSCs on RA.

Methods To compare their therapeutic efficacy, thapsigargin (TG)-stimulated or unstimulated MSCs were transplanted into collagen-induced arthritis (CIA) mice. Joint inflammation was evaluated from both general and histological aspects. Splenocytes were isolated, and flow cytometry was performed to assess the proportions of T helper 1 (Th1), Th17, and Tfh subsets. Additionally, the levels of TNF-*α* in mouse serum were measured using ELISA. For mechanistic exploration, the TRRUST and Cistrome Data Browser databases were used to analyse transcription factors related to COX2 regulation, as well as target genes regulated by activating transcription factor 4 (ATF4). To identify the most effective treatment concentration and duration for inducing ERS, we conducted a concentration and time gradient analysis for TG treatment via qRT–PCR and a CCK–8 assay. Then, western blotting and qRT–PCR were employed to determine the level of ATF4 in ERS-MSCs. To verify the function of ATF4 in vivo, ATF4-overexpressing MSCs were transplanted into CIA mice, the levels of joint inflammation as well as the proportions of Th1, Th17 and Tfh subsets were analysed. To clarify the molecular regulatory mechanism leading to ATF4 activation, the protein levels of protein kinase RNAs, such as endoplasmic reticulum kinase (PERK)/phosphorylated-PERK (p-PERK) and eukaryotic initiation factor 2*α* (eIF2*α*)/phosphorylated-eIF2*α* (p-eIF2*α*) were examined. Furthermore, the levels of ATF4 and eIF2*α*/p-eIF2*α* were assessed after PERK blockade. Mitochondrial stress was subsequently examined in ERS-MSCs. Finally, when blocking ERS and mitochondrial stress were inhibited separately or simultaneously, the levels of ATF4 and eIF2*α*/p-eIF2*α* were reevaluated.

[†]Jiaqing Liu and Xing Zhang have contributed equally to this work.

*Correspondence:
Weiping Li
liweiping0910@163.com
Jing Wei
weijingdl@126.com
Xia Li
lixia416@163.com

Results Compared with MSCs, ERS-MSCs exhibited greater therapeutic efficacy in CIA mice. Public databases and bioinformatics analyses confirmed the regulatory role of ATF4 in COX2, and experimental methods further demonstrated that ATF4-transfected MSCs alleviated joint inflammation in CIA mice. We also demonstrated that during ERS induction, PERK-mediated eIF2*α* phosphorylation contributes to the activation of ATF4. Furthermore, mitochondrial stress was also provoked in ERS-MSCs, and ERS synergistically regulated ATF4.

Conclusions Compared with unmodified MSCs, ERS-MSCs exhibited enhanced immunosuppressive potency, primarily through COX2 overexpression, which was regulated by ATF4 activation. Moreover, ERS and mitochondrial stress jointly regulated ATF4 expression. This study reveals a novel role of ATF4 in enhancing the secretory properties of MSCs and has thereby presents a promising MSC-based therapeutic strategy for the treatment of RA.

Keywords MSCs, ATF4, RA, Endoplasmic reticulum-mitochondria coupling stress

Introduction

Rheumatoid arthritis (RA) is characterized by persistent articular inflammation and synovitis, resulting in progressive cartilage degradation and structural joint damage. The global prevalence of RA is estimated to be approximately 5 cases per 1000 adults. Given its widespread impact on physical function and quality of life, RA imposes a significant burden on affected individuals and society as a whole [1]. Currently, conventional treatments for RA primarily involve corticosteroids, disease-modifying antirheumatic drugs (DMARDs), and biological agents, all of which are widely used in clinical practice. However, prolonged administration of these therapies is frequently limited by adverse drug reactions, and some RA patients may develop therapeutic resistance. Given these challenges, there is an urgent need for a more effective and sustainable alternative approach to RA treatment [1].

Mesenchymal stromal/stem cells (MSCs), as a valuable source for the treatment of immune-mediated disorders, are self-renewing, multipotent stem cells that possess the remarkable ability to regulate both innate and adaptive immune responses across nearly all adult tissues [2, 3]. MSC-based therapies have gained widespread application in the treatment of a variety of inflammatory diseases, due to their robust immunoregulatory capabilities [4]. In a randomized controlled trial conducted by Zeng et al., administration of MSCs was found to result in sustained improvements in clinical symptoms of rheumatic immune diseases, with notable effectiveness persisting for up to 12 months and achieving an overall clinical success rate of 54%. [5]. Furthermore, clinical studies have demonstrated that MSC therapy combined with DMARDs is not only safe but also provides sustained therapeutic benefits for RA patients. Notably, UC-MSCs in combination with DMARDs have shown particular promise in delivering long-term clinical improvements [6].

However, MSC-based therapies have encountered translational hurdles due to the decreased immunosuppressive capacities following cell delivery [7]. It has been proven that the phenotype, secretory profile, proliferative capacity, migratory ability, differentiation potential, and immunoregulatory functions of MSCs are all highly dependent on their local microenvironment. The soluble molecules released by MSCs are highly dependent on the host microenvironment, including factors such as inflammation status, hypoxia levels, and the composition of the extracellular matrix (ECM). This dependency results in highly variable factors that shape the plasticity of MSCs, thereby influencing their therapeutic efficacy and behavior [8]. Therefore, researchers are actively exploring innovative new strategies to enhance the immunosuppressive potency of MSCs in clinical applications [1]. In recent years, many approaches have been proposed to enhance the therapeutic efficacy of MSCs [9]. Current attempts to improve the therapeutic efficiency of MSCs were made mainly in the following aspects: engineering MSCs by viral transduction or CRISPR/Cas9 techniques for enhanced potency, or expansion capacities; priming MSCs with small molecules, hypoxia, or structural stimulations by biomaterials to improve MSC function and survival; bioengineering strategies to enhance MSC survival and functionality; utilizing the MSCs secretome mainly extracellular vesicles (EVs) as a natural drug carrier for more precise and sustained therapeutic effects through interactions with host cells [10]. Among these, pre-treated MSCs are easier to manipulate and have been studied in a variety of disease models [11, 12].

Endoplasmic reticulum (ER) is the site of biosynthesis for all secreted and membrane proteins. The accumulation of unfolded or misfolded proteins in ER can lead to ER stress (ERS). ERS functions as a double-edged sword: it can lead to apoptosis or induce changes in cellular function, theraby determining cell fate and survival [13]. Disruption of ER homeostasis triggers the unfolded protein response (UPR) through activation of three key sensor proteins: protein kinase R-like endoplasmic

reticulum kinase (PERK), inositol-requiring enzyme 1α (IRE1α) and activating transcription factor 6 (ATF6) to restore equilibrium. Activated PERK phosphorylates eukaryotic initiation factor 2*α* (eIF2*α*), which prevents translation of most mRNAs by inhibiting the initiation complex [14, 15]. Concurrently, phosphorylation of eIF2α favors increased translation of selective mRNAs. One of the key proteins whose translation is increased is activating transcription factor 4 (ATF4), a principal regulator that plays a crucial role in the adaptation to stress through regulating the transcription of many genes [16].

Although the precise etiology of RA remains unclear, the differentiation of $CD4^+$ T lymphocytes into pathogenic $CD4^+$ T subsets plays a crucial role in RA pathogenesis [17, 18]. Some RA therapeutic medications have displayed ERS-modulating properties. It has been verified that ERS-modulating traditional Chinese medicines are potential new pharmaceutical drugs for RA clinical therapy [19]. Our previous results have shown that ERS-MSCs displayed better immunomodulatory effects on Tfh subsets from RA patients through elevated prostaglandin E2 (PGE2) secretion [18]. This study aimed at exploring the therapeutic effect of ERS-MSC on ameliorating the severity of arthritis in a mouse model of RA, together with the molecular mechanism of the higher expression of PGE2, which could provide preclinical experimental data for the development of new stem cell-based drugs for the treatment of RA.

Methods

Isolation, culture, and identification of hUCMSCs

Human Umbilical Cord Mesenchymal Stem Cells (hUCMSCs) were isolated from healthy donors who had given birth and signed informed consents according to protocols reported previously [20, 21]. The umbilical cord tissues were aseptically dissected into 1.0 mm^3 explants using sterile surgical blades, followed by three consecutive PBS washes and centrifugation at 1900 rpm for 6 min. The cells were then cultured in an incubator at 37 °C and 5% CO_2 concentration with DMEM/F12 (Meilunbio, China) consisting of 10% fetal bovine serum (FBS) (Thermo Fisher Scientific, USA), 100 U/mL penicillin (Solarbio, China), and 100 mg/mL streptomycin (Solarbio, China). The primary cells were harvested when the confluence reached 80% and further characterized by flow cytometry (Agilent, USA) using the following fluorescein-labeled antibodies: CD90-Perep, CD105-PE, CD45-FITC, CD34-APC, CD14-FITC, CD11b-APC, and HLA-DR-PE (eBioscience, USA). Isotype-matched control antibodies were used as methodological controls. After identification (Fig. S1), hUCMSCs were treated with TG for ERS induction and followed by verificaion of an ERS induction (data not shown), as mentioned previously [18]. Cells reaching the fifth passage were employed in the following experiments.

Animals, disease induction and treatment

Male adult DBA/1 mice at 6–8 weeks were purchased from Shanghai SLAC Laboratory Animals Company and housed under pathogen-free conditions at the Laboratory Animal Center of Dalian Medical University. After a one-week acclimation period, mice undergoing the disease induction protocol were administered intradermal tail injections of a prepared collagen/Complete Freund adjuvant (CFA, Chondrex, USA) emulsion containing 1 mg/ml bovine type II collagen (Chondrex, USA) and 2 mg/ml on experimental day 0. Mice received a subsequent intradermal tail booster injection on day 21 with emulsion containing 1 mg/ml bovine type II collagen and 2 mg/ml Incomplete Freund's adjuvant (IFA, Chondrex, USA).

The study included healthy control mice ($n = 5$), mice undergoing the disease induction protocol treated with vehicle alone that served as the positive disease control group ($n = 5$), and mice undergoing the disease induction protocol treated with once a week for 4 times totally of caudal-vein injection with 2×10^6 cells of either hUCMSCs group (CIA + hUCMSCs), ERS-hUCMSCs group (CIA + ERS-hUCMSCs) or pc-ATF4-hUCMSCs group (CIA + pc-ATF4-hUCMSCs) on day 24 after subsequent immunization with five mice in each group. MSC-based transplantation was initiated at the same time and was started following the first observable signs of disease activity as determined by disease activity score. For positive disease control group (collagen-induced arthritis, CIA), equal amount of PBS was administered at the same time with the MSCs transplanted group through caudal vein injection. Throughout the experimental period, all mice underwent systematic monitoring 2–3 times weekly, including measurements of body weight, paw thickness, and disease activity scores.

Disease activity scores were derived from the evaluation of clinical arthritis in all four limbs as reported by scoring system for evaluating of arthritis severity [22]. A severity score of 0–4 was determined for each limb by visual evaluation and agreement between two examiners. No evidence of erythema and swelling of the limb implied a severity score of 0, a score of 1 was assigned for erythema and mild swelling confined to the tarsals or ankle joint, a score of 2 indicated erythema and swelling extending from the ankle to the tarsals, 3 meant erythema and extending from the ankle to metatarsal joints and a score of 4 was designated for erythema and severe swelling of the entire limb ankylosis. The disease activity score was obtained as the sum of the severity score for each limb with a peak score of 16. On experimental day

49, all the mice were euthanized by CO_2 infusion in a CO_2 line-connected box at a gas infusion rate of 1.5–3.5 L/minute. Once the animals ceased respiration for 5–10 min, euthanasia was confirmed by cervical dislocation, and tissue samples were harvested for subsequent analysis. No anesthesia was used in animal experiments of this study. The work has been reported in line with the ARRIVE guidelines 2.0.

Cell transfection

Small interfering RNA (siRNA) targeting ATF4 (GenePharma, China), OMA1 (Sevenbiotech, China) and a non-targeting negative control (NC) from General Biosystems, China, were transiently transfected into hUCMSCs with Lipofectamine 2000 transfection reagent (Invitrogen, USA) in serum-free medium at a working concentration of 100 nM according to the manufacturer's protocol. qRT-PCR and western blot were performed to verify the transfection effect. Cells were analyzed 24 or 48 h post-transfection.

To establish ATF4-overexpressing hUCMSCs, a pcDNA3.1 vector containing a sequence targeting the human ATF4 gene, pcDNA3.1-ATF4 was constructed by GenePharma (China). GenePharma also provided the pcDNA3.1-NC, negative control, and Lipofectamine 2000 (Invitrogen, USA) to transfect hUCMSCs. After determining transfection efficiency, cells were collected at 24 or 48 h post-transfection for the subsequent studies. Primer sequences were listed in Table S1.

RNA isolation and quantitative real-time PCR

Total RNA was extracted from hUCMSCs using TRIzol reagent (AG scientific, China) and reverse transcribed to cDNA using 5× Master Mix II (Sevenbiotech, China) according to the manufacturer's protocols. qRT-PCR was performed with the SYBR-Green Master Mix (Sevenbiotech, China) in triplicate using the CFX96 Real-Time PCR Detection System (Bio-Rad, USA) with the conditions of 95 °C for 30 s, then 40 cycles of 95 °C for 5 s and 60 °C for 30 s. The RNA expression levels of the target genes were normalized to the internal reference gene GAPDH using $2^{-\triangle\triangle CT}$ analysis method. The primer sequences were listed in Table S2.

Western blot analysis

Western blot was performed as previously described [23]. The following primary antibodies were used: anti-p-eIF2α (1:1000, CST, USA), anti-eIF2α (1:1000, CST, USA), anti-p-PERK (1:1000, CST, USA), anti-PERK (1:1000, CST, USA), anti-ATF4 (1:1000, CST, USA), anti-OMA1 (1:1000, CST, USA), anti-MiD49 (1:1000, Proteintech, China), anti-MiD51 (1:1000, Proteintech, China), anti-p-DRP1 (1:1000, CST, USA), anti-DRP1 (1:1000, CST, USA), anti-MFN2 (1:1000, WANLEIBIO, China), anti-OPA1 (1:1000, CST, USA), anti-Fis1 (1:1000, Affinity), anti-β-actin (1:1000, CST, USA), and anti-GAPDH (1:3000, Beyotime, China). Fluorescent secondary antibody (1:20,000, LI-COR, USA) was also employed. The results were identified using the Odyssey CLx Infrared Scanner (Odyssey CLx, USA), and relative protein expression was calculated using ImageJ software. β-actin or GAPDH served as internal references.

Mitochondrial membrane potential detection

3×10^4 cells of hUCMSCs in 12-well plates were pre-incubated with or without 1 μM thapsigargin (TG, Sigma, Germany) for 24 h. Mitochondrial membrane potential was assessed with the Assay Kit from AAT Bioquest (USA). Centrifuge the cells and resuspend in the JC-10 working solution. Subsequently, the cells were incubated in a 37 °C, 5% CO_2 incubator for 30 min. Subsequently, complete medium was added for washing. Finally, flow cytometry was performed at 366 nm and 430 nm, and images were obtained through fluorescence microscope (Olympus BX53, Japan). hUCMSCs treated with FCCP (10 μM, Sigma, Germany) were used as a positive control, as previously described [24].

Flow cytometry analyses for $CD4^+$ T cell subsets

To detect $CD4^+$ T cell subsets in mouse spleen and RA patient's peripheral blood, lymphocytes were obtained from the mouse spleen after grinding and passing through a 200-mesh filter. Peripheral blood mononuclear cells (PBMCs) from RA patients were isolated using Ficoll-Hypaque (TBD, China), and $CD4^+$ T cells were sorted by magnetic beads (Miltenyi Biotec, Germany). Then $CD4^+$ T cells were co-cultured with different treated hUCMSCs (20: 1) in RPMI 1640 medium (Meilunbio, China) containing anti-CD3 (2 μg/mL, eBioscience, USA) and anti-CD28 (2 μg/mL, eBioscience, USA) for 3 days.

For Th1 and Th17 quantification, cells were pelleted by centrifugation and resuspended in 10% FBS RPMI-1640 medium with phorbol 12-myristate 13-acetate (200 ng/uL, Fcmacs Biotech, China), ionomycin (1 μg/ml, Fcmacs Biotech, China) and brefeldin A (5 μg/ml, eBioscience, USA) at 37 °C, 5% CO_2 for 4 h. Cells were washed twice with cold PBS and stained with anti-human CD4-PE (Biolegend, USA) or anti-mouse CD4-FITC (Biolegend, USA). After permeabilization with Cytofix/Cytoperm (BD Biosciences, USA), cells were stained with anti-human IFN-γ-APC (eBioscience, USA), anti-human IL-17 A-PE (eBioscience, USA) or anti-mouse IFN-γ-APC (Biolegend, USA), anti-mouse IL-17 A-PE (Biolegend, USA). Tfh cells were stained with anti-human CD4-PE, anti-human PD1-PE/Cyanine7 (Biolegend,

USA), anti-human CXCR5-APC (eBioscience, USA) or anti-mouse CD4-FITC, anti-mouse PD1-APC/Cyanine7 (Biolegend, USA), anti-mouse CXCR5-APC (Biolegend, USA).

Histological analysis and Immunohistochemistry staining

The mouse ankle joints and organs were stained as previously reported [25]. Ankles and organs were fixed, sectioned, and stained with hematoxylin–eosin (H&E, Solarbio, China), Safranin O-fast green (SO/FG, Solarbio, China). Histomorphological observation was performed with a microscope (BX53, Olympus, Japan). Vimentin, TNF-α, and IL-1β were detected through immunohistochemistry (IHC) following a series of procedures: antigen retrieval, addition of vimentin primary antibody (Proteintech, China) and IgG secondary antibody (ZSGP-BIO, China), and finally adding a detection reagent to localize the primary antibody as reported previously [26].

Measurements of cellular ATP

ATP levels in cells were measured using an ATP Assay Kit (Solarbio, China) following the manufacturer's protocol. About 1 million cells were seeded in 75 cm^2 flasks. After treatment, cells were lysed by ultrasonication, centrifuged at 10,000 g for 3 min at 4 °C, and the supernatant was used for ATP measurement. ATP content was determined colorimetrically at 340 nm using a Microplate Reader (Thermo Fisher Scientific, USA), and expressed as μM per million cells.

Measurement of superoxide anion levels with MitoSOX™ Red

hUCMSCs were washed with PBS and digested with trypsin. Then the cells were washed again and incubated with 5 μM MitoSOX™ Red probe at 37 °C and 5% CO_2 for 10 min. Following incubation, the cells were washed twice with PBS. Fluorescence of the MitoSOX™ Red probe was measured using a microplate reader at excitation/emission wavelengths of 510 nm and 590 nm, respectively.

Statistical analysis

All statistical analyses were made by using Prism software (version 5, GraphPad). All experiments were conducted independently at least three times, and the results were expressed as mean ± standard deviation (SD). The comparison between two groups was analyzed by Student's t-test. Statistical differences among multiple groups were analyzed by one-way analysis of variance (ANOVA). $P < 0.05$ was considered statistical significance.

Results

ERS-hUCMSCs are more effective in at alleviating joint inflammation in CIA mice than are untreated hUCMSCs

The immunosuppressive effect of MSCs can be enhanced by ERS-induction in vitro. To further investigate this potential therapeutic strategy, we firstexplored the efficacy of utilizing ERS-primed MSCs in the treatment of RA in vivo. A well-established CIA mouse model was used to evaluate the effects of ERS-hUCMSCs on joint inflammation. After the onset of arthritis on Day 24, the mice were injected intravenously with either hUCMSCs or ERS-hUCMSCs weekly for 4 weeks (Fig. 1A). CIA mice gained weight more slowly than control mice did (Ctrl). hUCMSC treatment (CIA + hUCMSCs) failed to result in a recovery of body weight. In contrast, ERS-hUCMSC treatment (CIA + ERS-hUCMSCs) resulted in partial weight recovery (Fig. 1B). Morphological observation of the CIA mice revealed that the ERS-hUCMSC-treated mice presented less severe paw swelling and had lower arthritis scores (Fig. 1C–E). Similarly, H&E, SO/FG, vimentin, TNF-α, and IL-1β staining revealed that, compared with hUCMSC treatment alone, ERS-hUCMSC treatment effectively alleviated joint damage and bone erosion, decreased synovial cell proliferation, and suppressed inflammation (Fig. 1F). In addition, as shown in Fig. 1G–I, compared with the hUCMSC-treated group, the ERS-hUCMSC-treated group presented stronger immunosuppressive effects on major subsets of $CD4^+$ T cells, including Th1, Th17 and Tfh cells derived from the spleens of CIA mice, and reduced levels of TNF-α in the serum of CIA mice (Fig. 1J). Furthermore, compared with untreated hUCMSCs, ERS-hUCMSCs decreased the proportions of RA-related peripheral Th1, Th17 and Tfh subsets more obviously (Fig. S2).

(See figure on next page.)

Fig. 1 Transplantation of ERS-hUCMSCs demonstrates better therapeutic efficacy compared to hUCMSCs in a mouse model of CIA. For the induction of ERS, hUCMSCs are treated with TG (1 μM, 6 h). **A** The schematic flowchart depicts the establishment and treatment timeline of CIA mice from Day 0 to Day 49 ($n = 5$). **B** Growth curve of body weight ($n = 5$). **C** Changes in paw thickness ($n = 5$). **D** Clinical scoring of arthritis symptoms in CIA ($n = 5$). **E** Photographs of representative paws captured at the end of the experiment ($n = 5$). **F** Representative images of histopathological changes in ankle joints are demonstrated by H&E staining, SO/FG staining, and IHC for vimentin, TNF-α, and IL-1β ($n = 5$). **G-I** Flow cytometry analysis of activation markers for Th1, Th17, and Tfh (IFN-γ, IL-17 A, PD-1, and CXCR5) within the $CD4^+$ T cell population isolated from the spleens of mice in the indicated group ($n = 5$), is performed on the terminal day following CIA induction. **J** Detection of TNF-α levels in mouse serum using ELISA. Data are presented as mean ± standard deviation (SD). Statistical significance is indicated as follows: $^*p < 0.05$, $^{**}p < 0.01$, and $^{***}p < 0.001$

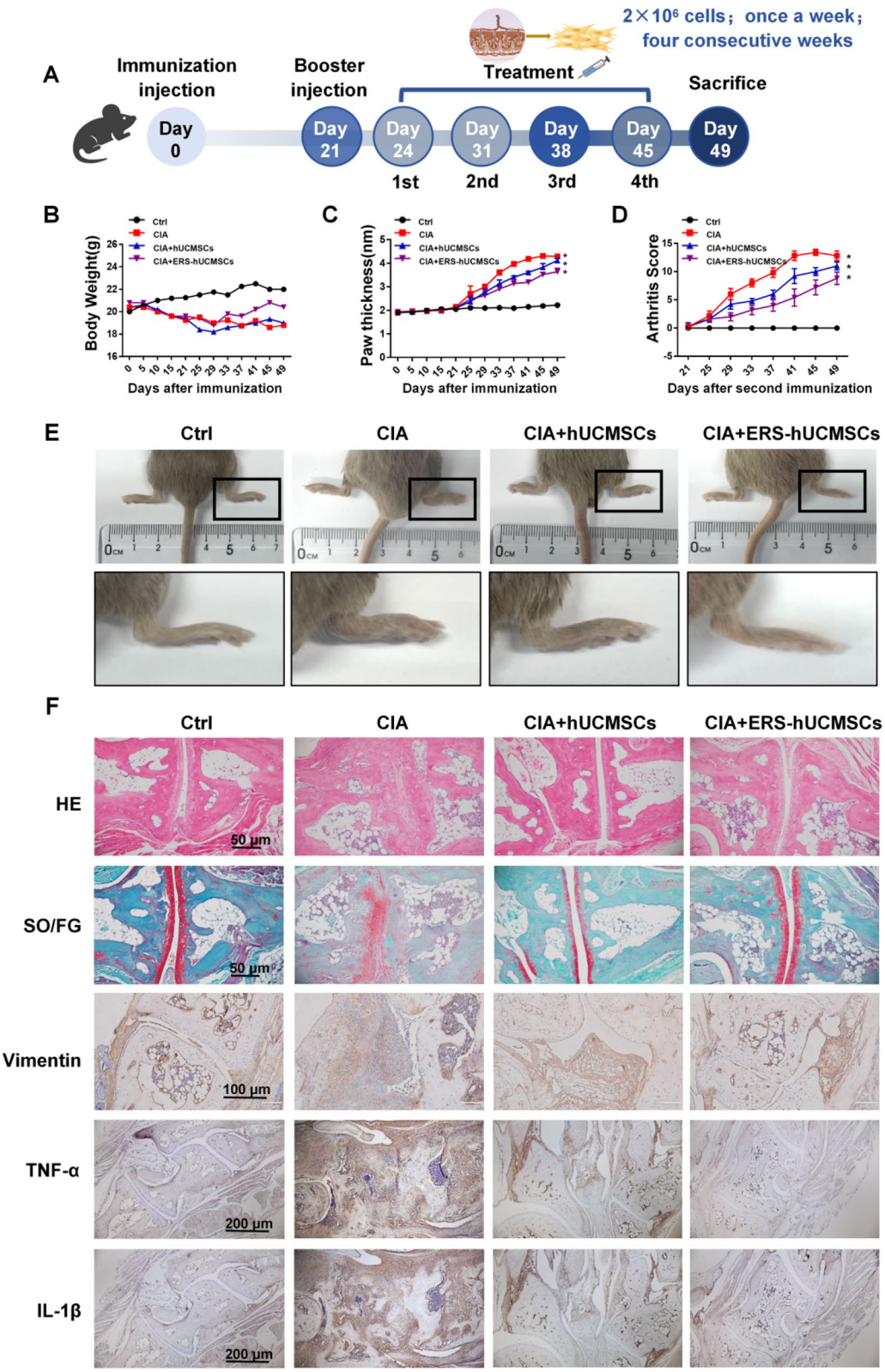

Fig. 1 (See legend on previous page.)

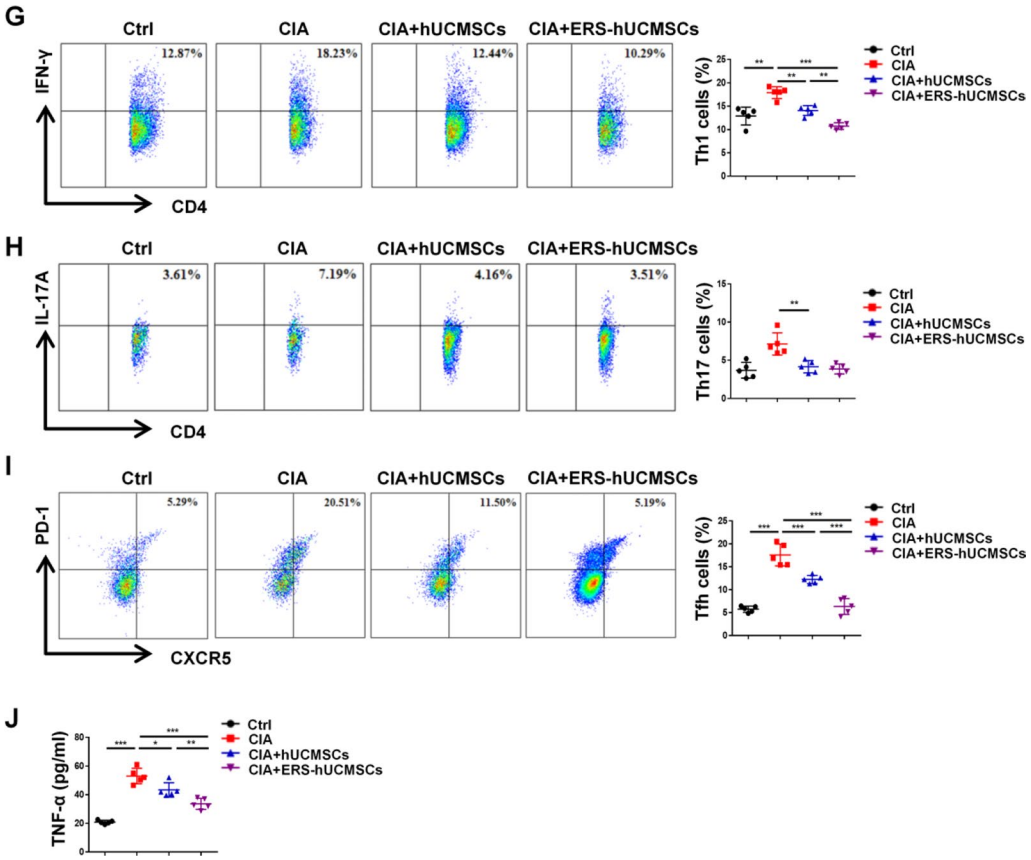

Fig. 1 continued

ATF4 is the key transcription factor regulating COX2 expression in ERS-hUCMSCs

We confirmed that ER-stressed MSCs exhibit enhanced immunosuppressive effects through cyclooxygenase-2 (COX2) overexpression, which increases PGE2 secretion [18]. We next investigated the transcription factor (TF) responsible for COX2 transcriptional regulation in ERS-hUCMSCs. First, we searched the TRRUST database for TFs related to COX2 regulation and identified 58 TFs. Among them, ATF4 has attracted our attention for its link with cellular stress in many cell lines [27], as it is also one of the signaling molecules related to ERS (Fig. 2A left).

We subsequently predicted the target genes regulated by ATF4 from both the TRRUST database and the Cistrome Data Browser database with OmicStudio tools. Initially, several target genes regulated by ATF4 were screened from the TRRUST database. After eliminating 6 duplicate genes, 35 target genes were ultimately identified. A search of the Cistrome Data Browser database yielded 100 distinct target genes regulated by ATF4, with no duplicates. Upon comparing the data from the two databases, the analysis revealed that COX2 was one of the potential target genes regulated by ATF4 (Fig. 2A right).

To identify the optimal concentration and duration for inducing ERS while minimizing cytotoxicity, we conducted a comprehensive analysis of TG treatment, examining concentration gradients and exposure durations (Fig. S3). Furthermore, during ERS, ATF4 levels were significantly elevated at both the mRNA and protein levels (Fig. 2B). Knockdown of ATF4 using specific siRNAs reduced basal COX2 levels under ERS conditions (Fig. 2C, D). Conversely, overexpression of ATF4 significantly increased COX2 mRNA expression (Fig. 2E, F). These findings suggested that ATF4 might be a key TF responsible for the upregulation of COX2 expression (Fig. 2G).

ATF4 overexpression enhances the immunomodulatory properties of hUCMSCs in CIA mice

To elucidate the in vivo function of ATF4, hUCMSCs overexpressing ATF4 (pc-ATF4-hUCMSCs) were transplanted into CIA mice at a dose of 2×10^6 cells per week for four consecutive weeks. Morphological observation of the CIA mice revealed that those treated with

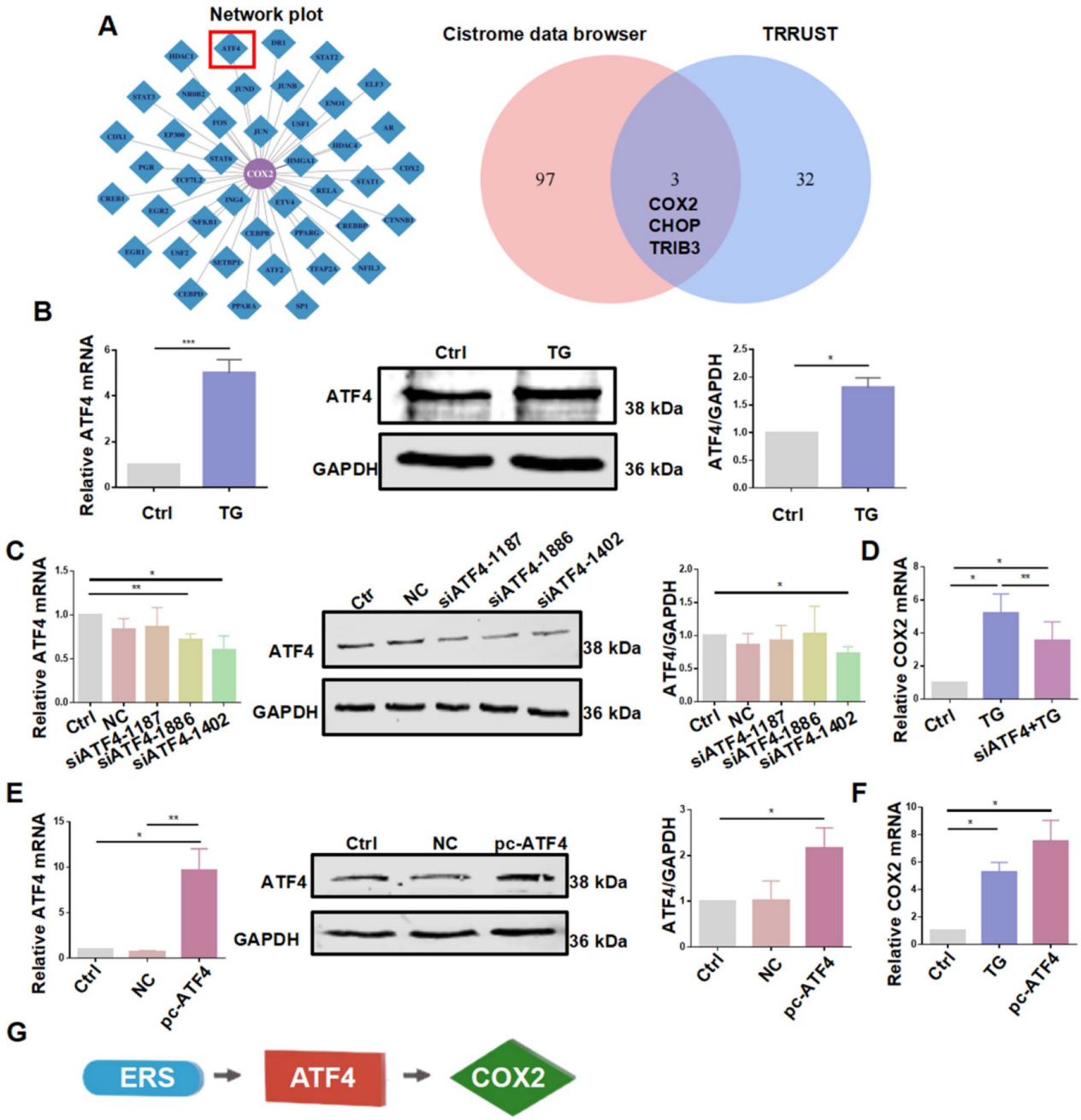

Fig. 2 ATF4 positively regulates COX2 expression in ERS induced hUCMSCs. **A** The TRRUST and Cistrome Data Browser databases are employed to identify transcription factors involved in the regulation of COX2, as well as target genes regulated by ATF4. **B** mRNA and protein levels of ATF4 in TG treated or un-treated groups ($n = 3$). Full-length blots are presented in Fig. S5 A. **C-F** mRNA levels of COX2 in hUCMSCs transfected with ATF4 knockdown or ATF4 overexpression. **C.** mRNA and protein levels of ATF4 following transfection with different siRNAs, using qRT-PCR at 24 h and Western blot at 48 h, respectively. siRNA, small interfering RNA; NC, negative control ($n = 3$). Full-length blots are presented in Supplementary Fig. S5B. **D** mRNA levels of COX2 under TG-stimulation in ATF4-knockdown conditions ($n = 3$). **E** mRNA and protein levels of ATF4 following transfection with an overexpression plasmid, using qRT-PCR at 24 h and Western blot at 48 h, respectively. pc-ATF4, plasmid construct-ATF4; NC, negative control ($n = 3$). Full-length blots are presented in Fig. S5C. **F** mRNA levels of COX2 under TG-stimulation or ATF4 overexpression conditions ($n = 3$). **G** ERS-hUCMSCs up-regulated COX2 expression through ATF4. Data are presented as the means ± SD from three independent experiments. Statistical significance is indicated as follows: $^{*}p < 0.05$, $^{**}p < 0.01$, and $^{***}p < 0.001$

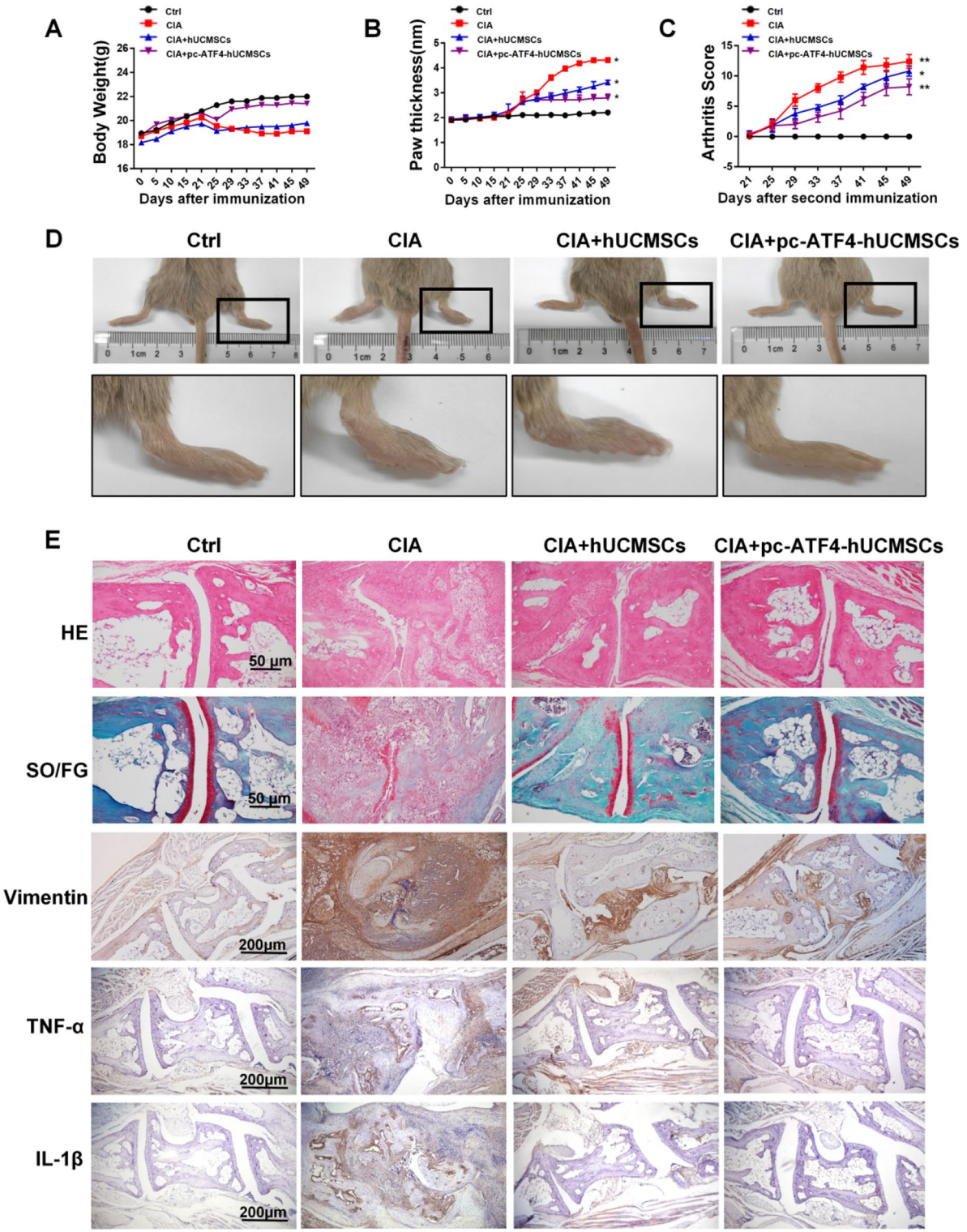

Fig. 3 Therapeutic effects of pc-ATF4-hUCMSCs transplantation in CIA mice model. A decrease in severity of CIA following pc-ATF4-hUCMSCs transplantation is demonstrated by body weight (**A**, $n = 5$), paw thickness (**B**, $n = 5$), and arthritis index scores (**C**, $n = 5$). Pictures of representative paws swelling (**D**), H&E, SO/FG stainings and subsequent histological examination of vimentin, TNF-α and IL-1β are performed at the end of the experiment (**E,** $n = 5$). Detection of $CD4^+$ T subsets, including Th1 (**F**), Th17 (**G**), and Tfh (**H**) subpopulations in the spleens of mice from indicated groups ($n = 5$). Data are presented as mean ± standard deviation (SD). Statistical significance is indicated as follows: $^*p < 0.05$, $^{**}p < 0.01$, and $^{***}p < 0.001$

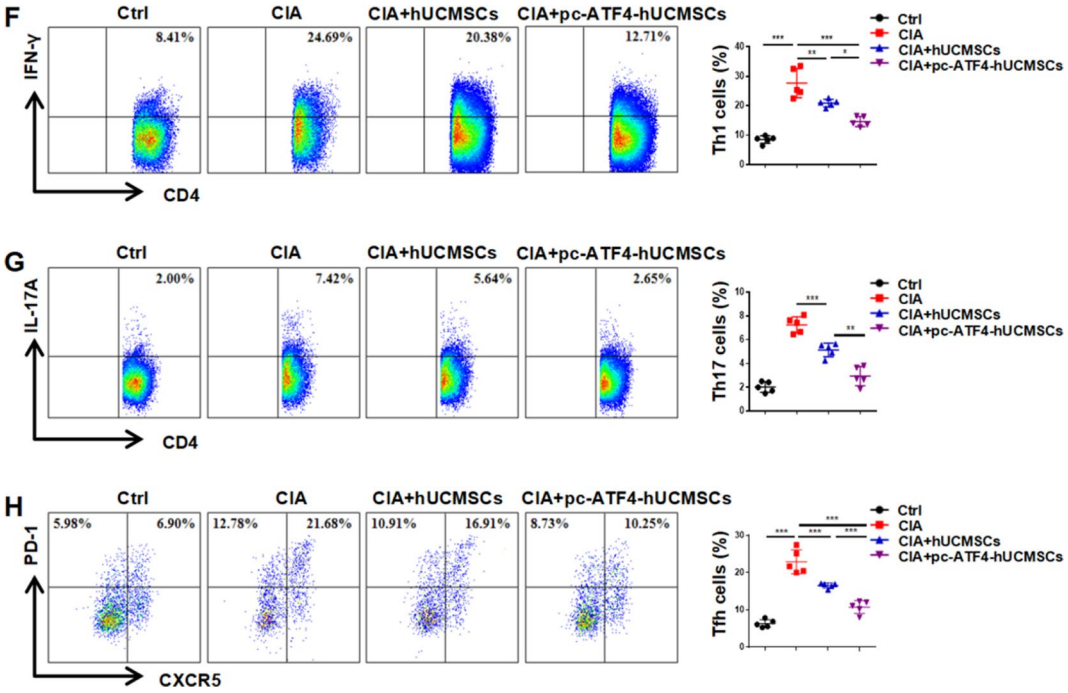

Fig. 3 continued

pc-ATF4-hUCMSCs presented greater stable body weights, less severe paw swelling, and lower arthritis scores than the control mice did (Fig. 3A–D). In addition, histological assessments using H&E staining, SO/FG staining, and immunohistochemical staining for vimentin, TNF-α, and IL-1β, demonstrated that compared with hUCMSC treatment alone, pc-ATF4-hUCMSC treatment significantly ameliorated joint damage and bone erosion (Fig. 3E). Moreover, compared with hUCMSC-treated cells, pc-ATF4-hUCMSCs had a stronger immunosuppressive effect on major subsets of $CD4^+$ T cells, including Th1, Th17, and Tfh cells (Fig. 3F–H). Moreover, compared with untreated hUCMSCs ($CD4^+$ T +hUCMSCs) and siATF4-hUCMSCs ($CD4^+$ T +siATF4), pc-ATF4-hUCMSCs ($CD4^+$ T +pc-ATF4) decreased the proportions of Th1, Th17, and Tfh subsets in the peripheral blood of RA patients (Fig. S4).

PERK-mediated eIF2α phosphorylation promotes the overexpression of ATF4

Given that ATF4 primarily contributes to the transcriptional regulation of COX2, we further explored the signaling pathways upstream of ATF4 in the context of ERS. Protein synthesis is controlled at several levels, with translation initiation being the foremost step [28]. Upon activation, the ERS response often inhibits translation initiation to restore cellular homeostasis. A key regulatory factor in this process is eIF2α, whose phosphorylation on serine at 51 leads to the inhibition of translation initiation. This prompted us to first examine the phosphorylation status of eIF2α. Our results revealed that eIF2α phosphorylation was significantly increased upon induction of ERS (Fig. 4A).

We continued to explore the factors contributing to eIF2α phosphorylation induced by ERS. There are 4 different upstream kinases of eIF2α: HRI, PKR, PERK, and GCN2 [29, 30]. Among them, PERK is established as a

(See figure on next page.)

Fig. 4 PERK-mediated eIF2α phosphorylation in hUCMSCs induced by ERS is essential for ATF4 upregulation. **A** Representative Western blot results are obtained using antibodies targeting p-eIF2α, total eIF2α, p-PERK, total PERK, and β-actin ($n = 3$). Full-length blots are presented in Fig. S6 A. **B** Protein levels of ATF4, p-eIF2α, total eIF2α, and β-actin in ERS-hUCMSCs in the presence or absence (control medium) of the PERK inhibitor, GSK2606414 (GSK, 1 μM, $n = 3$). Full-length blots are presented in Fig. S6B. **C** Protein levels of p-PERK, total PERK, p-eIF2α, total eIF2α and β-actin in ERS-hUCMSCs with or without GSK ($n = 3$). Full-length blots are presented in Fig. S6 C. Protein bands intensity is quantified by ImageJ. **D** Schematic diagram of the specific mechanism by which ATF4 is regulated by ERS. Data are indicated as means ± SD from three independent experiments. Statistical significance is indicated as follows: $^*p < 0.05$, $^{**}p < 0.01$, $^{***}p < 0.001$

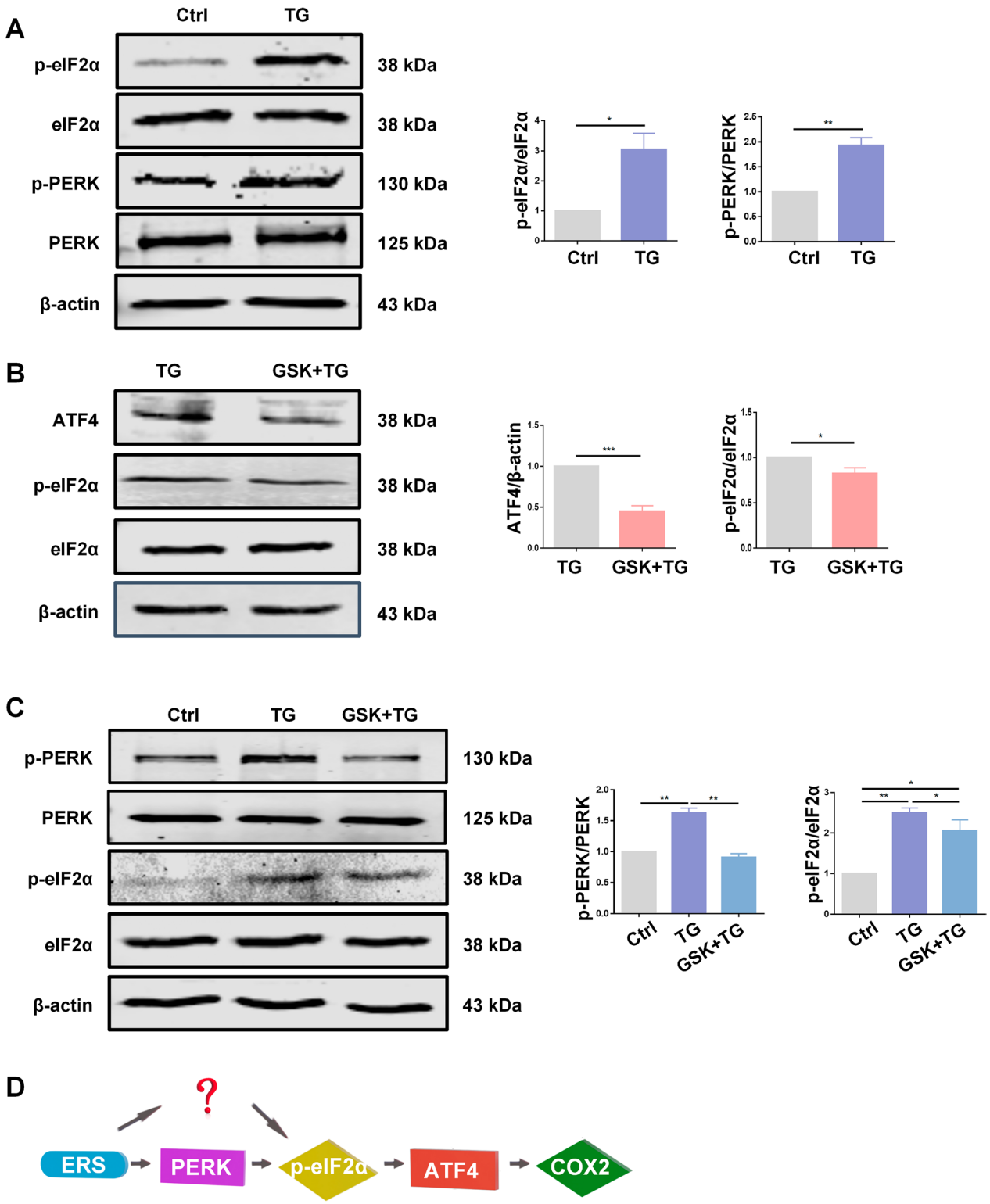

Fig. 4 (See legend on previous page.)

key marker involved in the ERS state [31]. As shown in Fig. 4A, both PERK and eIF2α were phosphorylated during the induction of ERS. Additionally, GSK2606414 (GSK), a potent inhibitor of PERK, downregulated the expression of ATF4 and the phosphorylation of eIF2α during ERS induction. This finding implies that PERK regulates ATF4 expression through the phosphorylation of eIF2*α* (Fig. 4B). To further validate this conclusion, a blank control group was included in the experiment. After treatment with GSK, the phosphorylation level of eIF2*α* was lower than that in the TG-treated group, but interestingly, it remained higher than that in the control (Ctrl) group (Fig. 4C), illustrating that eIF2*α* remained activated under ERS conditions even in the presence of PERK blockade (Fig. 4D).

ERS coupled with mitochondrial stress co-regulates ATF4 expression

Since the ER is in close contact with mitochondria through mitochondria-associated membranes (MAMs), ERS may be intertwined with mitochondrial function. We observed that overlap with m-AAA protease (OMA1), a major mitochondrial factor involved in sensing and responding to cellular stress, tended to increase as ERS increased (Fig. 5A). In addition, we evaluated mitochondrial dysfunctions, which are closely related to mitochondrial stress. After 24 h of TG stimulation, a decreased mitochondrial membrane potential (MMP), as indicated by JC-10 staining, was observed, with FCCP serving as a positive control for depolarization. Additionally, the NADH/NAD^+ ratio increased, ATP levels rose, and the mitochondrial $O_2^{\cdot -}$ content decreased (Fig. 5B).

Proteins involved in mitochondrial fission (Fis1, DRP1/p-DRP1, MiD49 and MiD51) and fusion (OPA1, MFN1, MFN2) were subsequently identified during ERS induction. The results revealed that phosphorylated dynamin-related protein 1 (DRP1) on Serine 616, mitochondrial fission 1 protein (Fis1), and mitochondrial dynamics protein of 51 kDa (MiD51) were downregulated, whereas mitochondrial dynamics protein of 49 kDa (MiD49) was upregulated. Additionally, the expression of mitofusin-2 (MFN2) decreased. Crucially, optic atrophy-1 (OPA1) directly links mitochondrial structure and function. As shown in Fig. 5C, when the mitochondrial membrane potential (ΔΨm) is lost, the long OPA1 isoforms (L-OPA1) are cleaved into short forms. This limits mitochondrial fusion and facilitates mitochondrial fission. These data illustrate that alterations in mitochondrial fission and fusion can be detected during ER stress induction, implying that mitochondrial stress is also induced during TG stimulation.

To further validate the role of mitochondrial stress in the upregulation of ATF4, we transfected hUCMSCs with siRNA targeting OMA1 (Fig. 6A). As shown in Fig. 6B, under ERS induction, simultaneous blockade of PERK and mitochondrial stress by GSK or siOMA1, respectively, had advantages over blockade alone in the downregulating ATF4, which implies that ERS and mitochondrial stress synergistically regulate ATF4 (Fig. 7).

Discussion

Our previous research demonstrated that ERS-induced hUCMSCs more effectively inhibited RA Tfh cells by releasing PGE2 [18], suggesting that the immunosuppressive capacity of hUCMSCs can be enhanced by ERS induction. The present study demonstrated, for the first time, that ATF4 plays a critical role in enhancing the effects of MSC-based therapy for RA through both ERS and mitochondrial stress. We observed that both the PERK-eIF2*α*-ATF4 signaling pathway from ERS and the OMA1-eIF2*α*-ATF4 signaling pathway triggered by mitochondrial stress were involved in COX2 regulation. The distinctive feature of our research lies in the method for processing MSCs, which is simple, easy to operate, and inexpensive. Under the premise of ensuring safety, the effectiveness of MSC-based therapy has increased.

ATF4, a cellular stress-induced transcription factor, regulates a variety of genes involved in various physiological processes and plays a critical role in stress responses. It orchestrates cellular responses, particularly in managing ERS [32, 33]. Research in reproduction has verified that ATF4 plays a unique role in COX2 regulation. It can bind to the COX2 promoter region and directly modulate COX2 expression [34]. COX2, which converts arachidonic acid into prostaglandins such as PGE2, is upregulated in response to ER stress. Elevated

(See figure on next page.)

Fig. 5 Mitochondrial stress is induced in ERS-hUCMSCs. **A** Protein levels of OMA1 from control and TG-treated hUCMSCs are measured over time ($n = 3$). Full-length blots are presented in Fig. S7 A. **B** Observation of mitochondrial membrane potential in cells using fluorescence and flow cytometry ($n = 4$). Detection of the NADH/NAD^+ratio, intracellular ATP levels, and mitochondrial $O_2^{\cdot -}$ content in cells with or without TG stimulation ($n = 3$). **C** Western blot analysis of mitochondrial dynamics-related proteins, including mitochondrial fission proteins, Fis1, MiD49, MiD51, p-DRP1 and DRP1 (left), and the mitochondrial fusion proteins, OPA1 and MFN2 (right) ($n = 3$). Protein levels in each group are relative to the control group. Full-length blots are presented in Fig. S7B. All values are shown as the means ± SD from three independent studies. Statistical significance is indicated as follows: $^*p < 0.05$, $^{**}p < 0.01$, $^{***}p < 0.001$

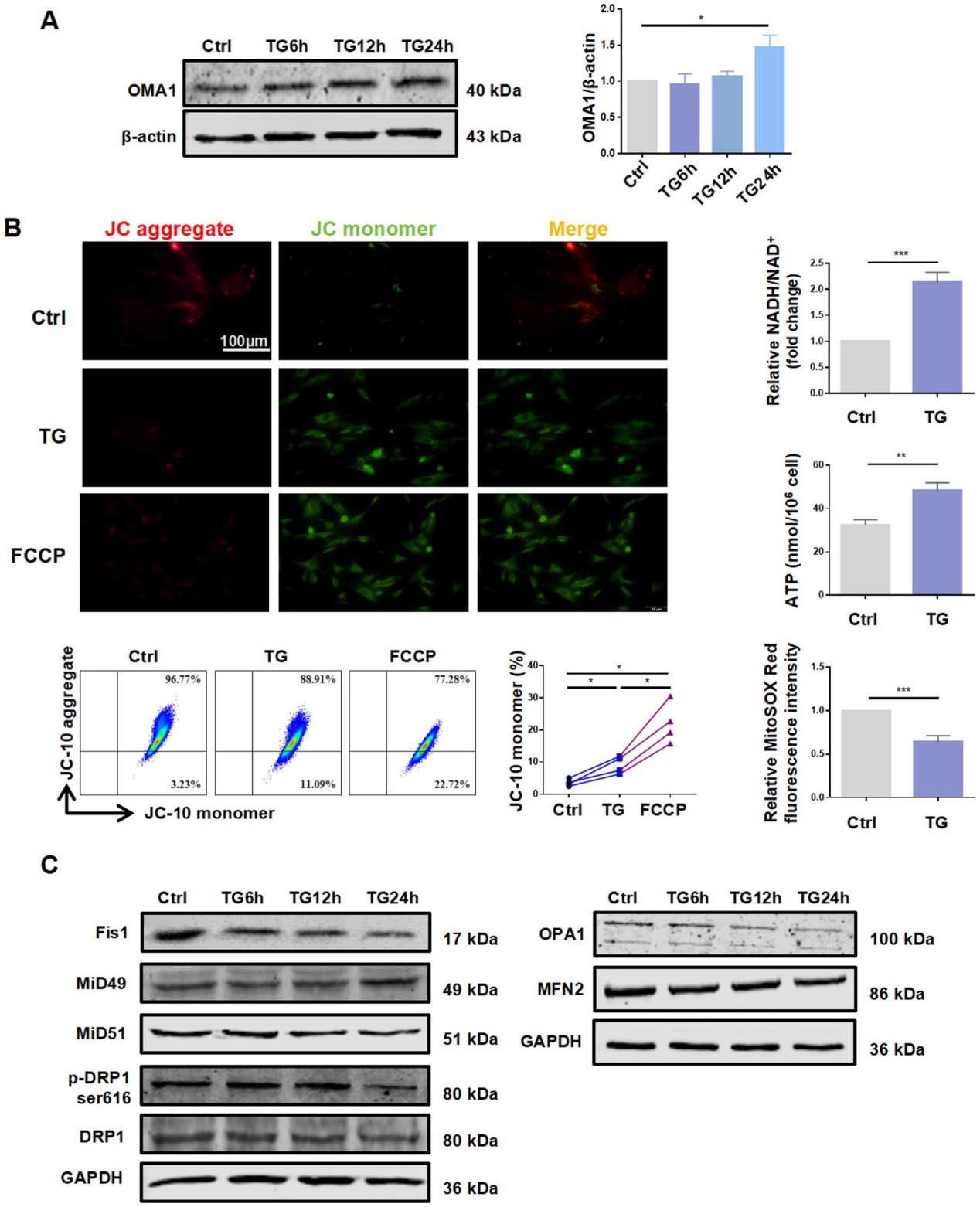

Fig. 5 (See legend on previous page.)

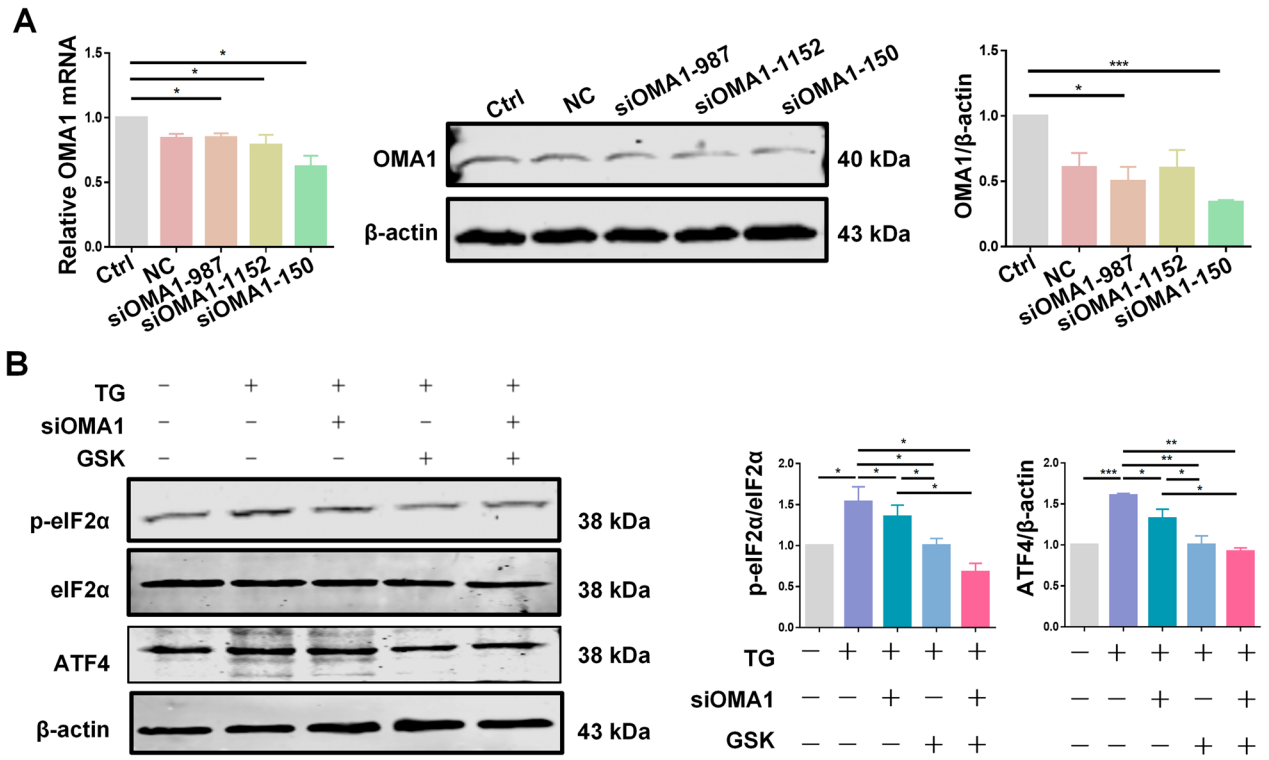

Fig. 6 ERS-integrated mitochondrial stress synergistically regulates ATF4. **A** Interference effect of OMA1 from both mRNA (left) and protein (right) levels ($n = 3$). Full-length blots are presented in Fig. S8A. **B** Western blot analysis of p-eIF2α, eIF2α and ATF4 in hUCMSCs transfected with siRNA targeting OMA1 and treated with GSK or TG ($n = 3$). Full-length blots are presented in Fig. S8B. Data are indicated as means ± SD from three independent experiments. Statistical significance is indicated as follows: $^{*}p < 0.05$, $^{**}p < 0.01$, $^{***}p < 0.001$

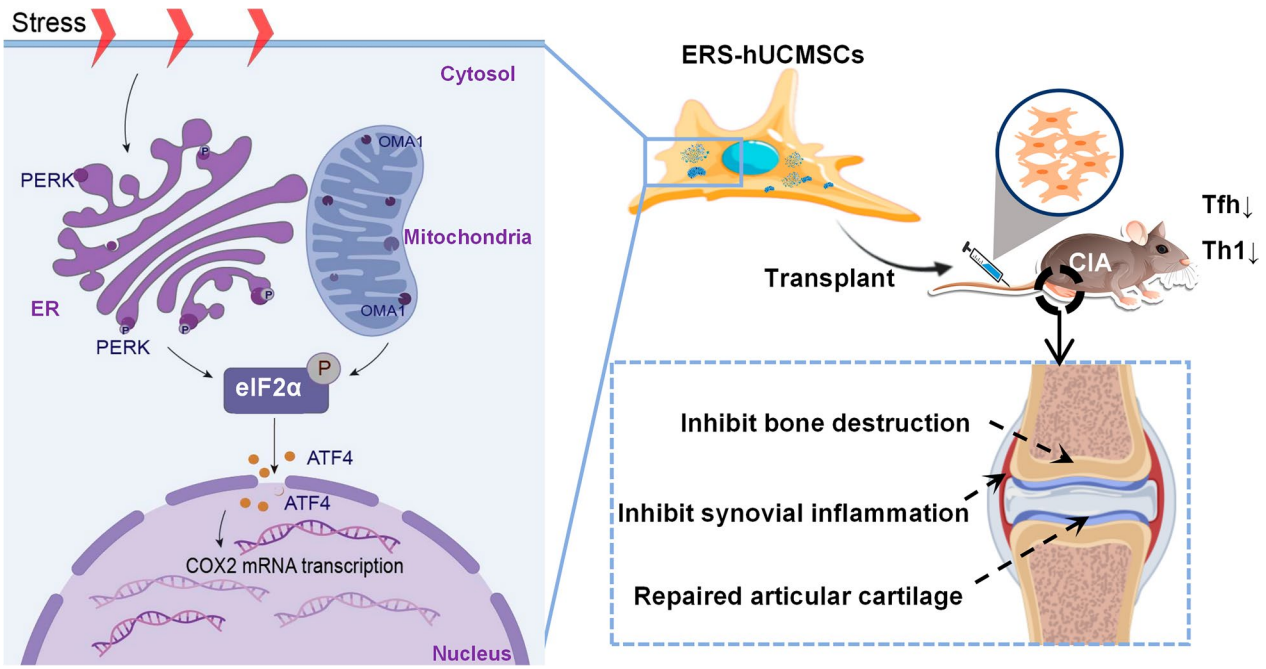

Fig. 7 A proposed model illustrating how endoplasmic reticulum stress (ERS) enhances the therapeutic effect of mesenchymal stem cells (MSCs) during rheumatoid arthritis (RA) treatment

COX2 levels increase PGE2 production, which inhibits T-cell receptor signaling and thereby limits T-cell activation [16]. Moreover, cadmium-induced overexpression of COX2, which is dependent on ATF4 transcriptional regulation, also occurs in the context of ERS [35].

The ER is the main organelle related to protein synthesis, modification, calcium ions storage, and processing in eukaryotic cells [36]. Mounting evidence suggests that altered ER homeostasis leads to the accumulation of unfolded or misfolded proteins in the ER lumen, disrupting protein-folding homeostasis and creating a condition known as ERS [37–39]. In response to ERS, cytoprotective axes are triggered to restore protein homeostasis in the ER through the unfolded protein response (UPR), which initiates prosurvival or prodeath responses and determines cell fate via the induction of the PERK, ATF6 and IRE1 pathways [40].

The ER serves as the primary intracellular reservoir for calcium ions, while mitochondria rely on calcium ions to regulate their metabolic functions. ERS can lead to the release of calcium ions, which are subsequently transferred to mitochondria, causing mitochondrial calcium overload. Mitochondrial calcium overload further increases the production of reactive oxygen species (ROS), leading to mitochondrial oxidative stress [41]. The contact sites between the ER and mitochondria are known as MAMs. MAMs are physical and functional connections between the ER and mitochondria that influence cell survival and death by regulating the transfer of calcium ions and other metabolites. Thus, the mitochondria and the ER can regulate each other via MAMs [42, 43].

ERS and mitochondrial stress are implicated in a broad range of diseases beyond RA. In ischemia–reperfusion injury, ERS and mitochondrial stress act jointly on cardiomyocytes. IR injury induces ERS, which subsequently leads to mitochondrial calcium overload and excessive ROS production, ultimately triggering cardiomyocyte apoptosis [44]. ERS and mitochondrial dysfunction are among the core pathological mechanisms in some neurodegenerative diseases. For example, the accumulation of β-amyloid can induce ERS, while mitochondrial dysfunction leads to increased ROS production, which further exacerbates neuronal damage in Alzheimer's disease [45, 46]. Recent studies have revealed that the abnormal interactions between the ER and mitochondria are key factors in the development of nonalcoholic fatty liver disease and hepatic fibrosis [47]. ERS can support the proliferation of tumor cells by regulating mitochondrial metabolism, but excessive stress can also trigger apoptosis [48]. Our results demonstrate that ERS can induce mitochondrial stress, with eIF2α phosphorylation being the central event in the ER–mitochondrion coupling stress, ultimately leading to the activation of the transcription factor, ATF4. In this study, we further confirmed that during ERS, the upregulation of COX2 is dependent on ATF4. This increase in COX2 is closely linked to the cellular stress orchestrated by two pathways: the PERK-eIF2α-ATF4 axis of the UPR pathway and the OMA1-eIF2α-ATF4 axis of the mitochondrial stress response. Our research demonstrated that the ATF4 pathway, which is activated by both ERS and mitochondrial stress, increases COX2 expression, thereby increasing the therapeutic efficacy of MSC-based treatments.

This study has several limitations that should be elucidated. First, the translational challenges in applying findings from mouse models to humans represent a significant limitation. Second, the scalability of ERS-MSC preparation is another challenge. The currently employed methods for ERS-MSC preparation may not be easily scaled up for clinical applications, which restricts their potential use. Given these limitations, future research should focus on developing more human-relevant models, such as humanized mice or in vitro human tissue models, to better bridge the gap between preclinical and clinical studies. Furthermore, improving the scalability of ERS-MSC preparation through optimized culture conditions and bioprocess engineering will be crucial for advancing their clinical application. These efforts will increase the translational potential of our findings and contribute to the development of more effective therapeutic strategies.

Conclusions

In summary, our findings demonstrate that compared with unpretreated hUCMSCs, ER-stressed hUCMSCs exhibit increased immunosuppressive capacity, primarily through the overexpression of COX2, which is regulated by ATF4. ATF4 activation is coregulated by ERS and mitochondrial stress. ERS activates PERK-eIF2α, whereas mitochondrial stress activates OMA1-eIF2α, both of which contribute to the regulation of ATF4 expression.

Abbreviations

MSCs	Mesenchymal stem/stromal cells
ERS	Endoplasmic reticulum stress
RA	Rheumatoid arthritis
Tfh	Follicular helper T cells
COX2	Cyclooxygenase-2
PGE2	Prostaglandin E2
TG	Thapsigargin
CIA	Collagen-induced arthritis
Th1	T helper 1
Th17	T helper 17
ATF4	Activating transcription factor 4
PERK	Protein kinase R-like endoplasmic reticulum kinase
p-PERK	Phosphorylated-PERK
HRI	Heme-regulated inhibitor
PKR	Protein kinase R
GCN2	General control nonderepressible 2
eIF2α	Eukaryotic initiation factor 2α

p-eIF2α	Phosphorylated-eIF2*α*
ER	Endoplasmic reticulum
UPR	Unfolded protein response
IRE1α	Inositol-requiring enzyme 1α
ATF6	Activating transcription factor 6
hUCMSCs	Human umbilical cord mesenchymal stem cells
TF	Transcription factor
MAM	Mitochondria-associated membranes
OMA1	Overlap with m-AAA protease
MMP	Mitochondrial membrane potential
MiD51	Mitochondrial dynamics proteins of 51 kDa
MiD49	Mitochondrial dynamics proteins of 49 kDa
MFN2	Mitofusin-2
OPA1	Optic atrophy-1
L-OPA1	Long OPA1 isoforms

Supplementary Information

The online version contains supplementary material available at https://doi.org/10.1186/s13287-025-04362-x.

Supplementary material 1.

Supplementary material 2.

Supplementary material 3.

Acknowledgements
This work was supported by grants from the National Natural Science Foundation of China (82071834, 82271839), Liaoning Undergraduate Program for Innovation and Entrepreneurship (S202310161043, S202310161019), Dalian Medical University Interdisciplinary Research Cooperation Project Team Funding (JCHZ2023010), and Liaoning Provincial Education Department Basic Research Project (LJ212410161034, LJ212410161038). The authors solemnly declare that no content in this manuscript has been generated by artificial intelligence (AI). We extend our gratitude to all lab members for their insights and discussions throughout the research process.

Author contributions
Jiaqing Liu: Formal analysis, Investigation, Writing – review & editing. Xing Zhang: Formal analysis, Investigation, Methodology, Writing – original draft. Xiangge Zhao: Methodology, Writing – review & editing. Jinyi Ren: Formal analysis, Writing – review & editing. Huina Huang and Cheng Zhang: Formal analysis, Investigation, Writing – original draft. Xianmei Chen: Writing – review & editing. Weiping Li: Human tissue providing. Jing Wei: Article designing, Writing – drafting & revising. Xia Li: Project administration, Funding acquisition, Validation.

Funding
National Natural Science Foundation of China, 82071834, Xia Li,82271839, Xia Li, Liaoning Undergraduate Program for Innovation and Entrepreneurship, S202310161043, Jing Wei, Liaoning Undergraduate Program for Innovation and Entrepreneurship, S202310161019, Jing Wei, Liaoning Provincial Education Department Basic Research Project, LJ212410161034, Xia Li, Liaoning Provincial Education Department Basic Research Project, LJ212410161038, Jing Wei, Dalian Medical University Interdisciplinary Research Cooperation Project Team Funding, JCHZ2023010, Xia Li.

Availability of data and materials
All additional files have been included in the manuscript. Using the OmicStudio tools, it is possible to predict the target genes regulated by ATF4 in both the TRRUST database and the Cistrome Data Browser database.

Declarations

Ethics approval and consent to participate
All animal procedures were conducted in strict accordance with the guidelines established by the Experimental Animals Management Committee of Liaoning Province, China, and were approved by the Experimental Animals Welfare and Ethical Committee (Date:16. 05. 2024, No. AEE24013), Dalian Medical University. Project name: Research on Pathogenesis and Treatment of Autoimmune Diseases. Human MSCs and RA peripheral blood samples were obtained from consenting volunteers enrolled in this study at the Second Hospital of Dalian Medical University. This study was approved by the Ethics Committee of the Second Hospital of Dalian Medical University (Date: 08. 10. 2023, ethical approval number: 2023–253). Project name: Pathogenesis Research and Immunotherapy in Patients with Autoimmune Diseases.

Consent for publication
Not Applicable.

Competing interests
The authors declare that they have competing financial interests or personal relationships that could have influenced the work reported in this paper.

Author details
[1]Department of Immunology, College of Basic Medical Science, Dalian Medical University, Dalian 116044, Liaoning, China. [2]Department of Hematology, The Second Hospital of Dalian Medical University, Dalian 116600, Liaoning, China.

Received: 10 December 2024 Accepted: 23 April 2025
Published online: 28 May 2025

References

1. Sarsenova M, Issabekova A, Abisheva S, Rutskaya-Moroshan K, Ogay V, Saparov A. Mesenchymal stem cell-based therapy for rheumatoid arthritis. Int J Mol Sci. 2021;22:11592.
2. Wang Y, Fang J, Liu B, Shao C, Shi Y. Reciprocal regulation of mesenchymal stem cells and immune responses. Cell Stem Cell. 2022;29:1515–30.
3. Jiang B, Yao G, Tang X, Yang X, Feng X. MSCs relieve SLE by modulation of Th17 cells through MMPs–CCL2–CCR2–IL-17 pathway. Rheumatol Autoimmun. 2021;1:30–9.
4. Han Y, Yang J, Fang J, Zhou Y, Candi E, Wang J, et al. The secretion profile of mesenchymal stem cells and potential applications in treating human diseases. Signal Transduct Target Ther. 2022;7:92.
5. Zeng L, Liu C, Wu Y, Liu S, Zheng Y, Hao W, et al. Efficacy and safety of mesenchymal stromal cell transplantation in the treatment of autoimmune and rheumatic immune diseases: a systematic review and meta-analysis of randomized controlled trials. Stem Cell Res Ther. 2025;16(1):65.
6. Wang L, Huang S, Li S, Li M, Shi J, Bai W, Wang Q, Zheng L, Liu Y. Efficacy and safety of umbilical cord mesenchymal stem cell therapy for rheumatoid arthritis patients: a prospective phase I/II study. Drug Des Devel Ther. 2019;13:4331–40.
7. Maji S, Aliabouzar M, Quesada C, Chiravuri A, Macpherson A, Pinch A, et al. Ultrasound-generated bubbles enhance osteogenic differentiation of mesenchymal stromal cells in composite collagen hydrogels. Bioact Mater. 2024;43:82–97.
8. Zhou T, Yuan Z, Weng J, Pei D, Du X, He C. Challenges and advances in clinical applications of mesenchymal stromal cells. J Hematol Oncol. 2021;14(1):24.
9. Alagesan S, Brady J, Byrnes D, Fandiño J, Masterson C, McCarthy S, et al. Enhancement strategies for mesenchymal stem cells and related therapies. Stem Cell Res Ther. 2022;13:75.
10. Boysen AT, Whitehead B, Revenfeld ALS, Gupta D, Petersen T, Nejsum P. Urine-derived stem cells serve as a robust platform for generating native or engineered extracellular vesicles. Stem Cell Res Ther. 2024;15(1):288.
11. Sarsenova M, Kim Y, Raziyeva K, Kazybay B, Ogay V, Saparov A. Recent advances to enhance the immunomodulatory potential of mesenchymal stem cells. Front Immunol. 2022;13:1010399.
12. Zhang Z, Cui Y, Huang S, Liu W, Chen C, Feng X, et al. Enhanced therapeutic effects of apoptotic cell-conditioned mesenchymal stem cells in lupus-prone MRL/lpr mice. Rheumatol & Autoimmun. 2024;4:90–8.
13. Chen X, Cubillos-Ruiz JR. Endoplasmic reticulum stress signals in the tumour and its microenvironment. Nat Rev Cancer. 2021;21:71–88.
14. Marciniak SJ, Chambers JE, Ron D. Pharmacological targeting of endoplasmic reticulum stress in disease. Nat Rev Drug Discov. 2022;21:115–40.

15. Chen Z, Tian R, She Z, Cai J, Li H. Role of endoplasmic reticulum stress in the pathogenesis of nonalcoholic fatty liver disease. Free Radic Biol Med. 2020;152:116–41.
16. Pandey VK, Mathur A, Khan MF, Kakkar P. Activation of PERK-eIF2α-ATF4 pathway contributes to diabetic hepatotoxicity: attenuation of ER stress by Morin. Cell Signal. 2019;59:41–52.
17. Wang M, Xue Y, Du F, Ma L, Lu LJ, Jiang L, et al. Continuation, reduction, or withdrawal of tofacitinib in patients with rheumatoid arthritis achieving sustained disease control: a multicenter, open-label, randomized controlled trial. Chin Med J (Engl). 2023;136:331–40.
18. Wei J, Ouyang X, Tang Y, Li H, Wang B, Ye Y, et al. ER-stressed MSC displayed more effective immunomodulation in RA CD4(+)CXCR5(+) ICOS(+) follicular helper-like T cells through higher PGE2 binding with EP2/EP4. Mod Rheumatol. 2020;30:509–16.
19. de Seabra Rodrigues Dias IR, Lo HH, Zhang K, Law BYK, Nasim AA, Chung SK, et al. Potential therapeutic compounds from traditional Chinese medicine targeting endoplasmic reticulum stress to alleviate rheumatoid arthritis. Pharmacol Res. 2021;170:105696.
20. Zhao C, Zhang L, Kong W, Liang J, Xu X, Wu H, et al. Umbilical cord-derived mesenchymal stem cells inhibit cadherin-11 expression by fibroblast-like synoviocytes in rheumatoid arthritis. J Immunol Res. 2015;2015: 137695.
21. Xiang E, Han B, Zhang Q, Rao W, Wang Z, Chang C, et al. Human umbilical cord-derived mesenchymal stem cells prevent the progression of early diabetic nephropathy through inhibiting inflammation and fibrosis. Stem Cell Res Ther. 2020;11:336.
22. Brand DD, Latham KA, Rosloniec EF. Collagen-induced arthritis. Nat Protoc. 2007;2:1269–75.
23. Wei J, Huang X, Zhang X, Chen G, Zhang C, Zhou X, et al. Elevated fatty acid β-oxidation by leptin contributes to the proinflammatory characteristics of fibroblast-like synoviocytes from RA patients via LKB1-AMPK pathway. Cell Death Dis. 2023;14:97.
24. Klier PEZ, Martin JG, Miller EW. Imaging reversible mitochondrial membrane potential dynamics with a masked rhodamine voltage reporter. J Am Chem Soc. 2021;143:4095–9.
25. Lin WW, Ho KW, Su HH, Fang TF, Tzou SC, Chen IJ, et al. Fibrinogen-Like protein 1 serves as an anti-inflammatory agent for collagen-induced arthritis therapy in mice. Front Immunol. 2021;12: 767868.
26. Magaki S, Hojat SA, Wei B, So A, Yong WH. An introduction to the performance of immunohistochemistry. Methods Mol Biol. 2019;1897:289–98.
27. Wortel IMN, van der Meer LT, Kilberg MS, van Leeuwen FN. Surviving stress: modulation of ATF4-mediated stress responses in normal and malignant cells. Trends Endocrinol Metab. 2017;28:794–806.
28. Lomakin IB, Steitz TA. The initiation of mammalian protein synthesis and mRNA
29. Wen W, Zhao Q, Yin M, Qin L, Junjie H, Chen H, Li X, Qian P. Seneca valley virus 3C protease inhibits stress granule formation by disrupting eIF4GI-G3BP1 interaction. Front Immunol. 2020. https://doi.org/10.3389/fimmu.2020.577838.
30. Guo X, Aviles G, Liu Y, Tian R, Unger BA, Lin YT, et al. Mitochondrial stress is relayed to the cytosol by an OMA1-DELE1-HRI pathway. Nature. 2020;579:427–32.
31. Zeng T, Zhou Y, Yu Y, Wang JW, Wu Y, Wang X, et al. rmMANF prevents sepsis-associated lung injury via inhibiting endoplasmic reticulum stress-induced ferroptosis in mice. Int Immunopharmacol. 2023;114: 109608.
32. Tang H, Kang R, Liu J, Tang D. ATF4 in cellular stress, ferroptosis, and cancer. Arch Toxicol. 2024;98:1025–41.
33. Neill G, Masson GR. A stay of execution: ATF regulation and potential outcomes for the integrated stress response. Front Mol Neurosci. 2023;16:1112253.
34. Di F, Liu J, Li S, Yao G, Hong Y, Chen ZJ, et al. ATF4 contributes to ovulation via regulating COX2/PGE2 expression: a potential role of ATF4 in PCOS. Front Endocrinol (Lausanne). 2018;9:669.
35. Luo B, Lin Y, Jiang S, Huang L, Yao H, Zhuang Q, et al. Endoplasmic reticulum stress eIF2α-ATF4 pathway-mediated cyclooxygenase-2 induction regulates cadmium-induced autophagy in kidney. Cell Death Dis. 2016;7: e2251.
36. Hughes A, Oxford AE, Tawara K, Jorcyk CL, Oxford JT. Endoplasmic reticulum stress and unfolded protein response in cartilage pathophysiology; contributing factors to apoptosis and osteoarthritis. Int J Mol Sci. 2017;18:665.
37. Hetz C, Papa FR. The unfolded protein response and cell fate control. Mol Cell. 2018;69:169–81.
38. Hetz C, Chevet E, Oakes SA. Proteostasis control by the unfolded protein response. Nat Cell Biol. 2015;17:829–38.
39. Karagoz GE, Acosta-Alvear D, Walter P. The unfolded protein response: detecting and responding to fluctuations in the protein-folding capacity of the endoplasmic reticulum. Cold Spring Harb Perspect Biol. 2019;11: a033886.
40. Kasahara A, Scorrano L. Mitochondria: from cell death executioners to regulators of cell differentiation. Trends Cell Biol. 2014;24:761–70.
41. Makio T, Chen J, Simmen T. ER stress as a sentinel mechanism for ER Ca2+ homeostasis. Cell Calcium. 2024;124: 102961.
42. He Q, Qu M, Shen T, Su J, Xu Y, Xu C, et al. Control of mitochondria-associated endoplasmic reticulum membranes by protein S-palmitoylation: novel therapeutic targets for neurodegenerative diseases. Ageing Res Rev. 2023;87: 101920.
43. Zhao WB, Sheng R. The correlation between mitochondria-associated endoplasmic reticulum membranes (MAMs) and Ca2+ transport in the pathogenesis of diseases. Acta Pharmacol Sin. 2025;46(2):271–91.
44. Wei J, Wu X, Luo P, Yue K, Yu Y, Pu J, et al. Homer1a attenuates endoplasmic reticulum stress-induced mitochondrial stress after ischemic reperfusion injury by inhibiting the PERK pathway. Front Cell Neurosci. 2019;13:101.
45. Calvo-Rodriguez M, Kharitonova EK, Snyder AC, Hou SS, Sanchez-Mico MV, Das S, et al. Real-time imaging of mitochondrial redox reveals increased mitochondrial oxidative stress associated with amyloid beta aggregates in vivo in a mouse model of Alzheimer's disease. Mol Neurodegener. 2024;19:6.
46. Costa RO, Ferreiro E, Martins I, Santana I, Cardoso SM, Oliveira CR, et al. Amyloid β-induced ER stress is enhanced under mitochondrial dysfunction conditions. Neurobiol Aging. 2012;33:824.
47. Dong J, Chen L, Ye F, Tang J, Liu B, Lin J, et al. Mic19 depletion impairs endoplasmic reticulum-mitochondrial contacts and mitochondrial lipid metabolism and triggers liver disease. Nat Commun. 2024;15(1):168.
48. Clarke HJ, Chambers JE, Liniker E, Marciniak SJ. Endoplasmic reticulum stress in malignancy. Cancer Cell. 2014;25(5):563–73.

Publisher's Note